Icarus 217 (2012) 115–129

Contents lists available at SciVerse ScienceDirect

Icarus

journal homepage: www.elsevier.com/locate/icarus

Ganymede crater dimensions – Implications for central peak and central pit formation and development

Veronica J. Bray [a,*], Paul M. Schenk [b], H. Jay Melosh [c], Joanna V. Morgan [d], Gareth S. Collins [d]

[a] Lunar and Planetary Laboratory, University of Arizona, Tucson, AZ 85721, USA
[b] Lunar and Planetary Institute, 3600 Bay Area Blvd., Houston, TX 77058, USA
[c] Department of Earth and Atmospheric Sciences, Purdue University, West Lafayette, IN 47907, USA
[d] Earth Science and Engineering Department, Imperial College London, Exhibition Road, London SW7 2BP, UK

ARTICLE INFO

Article history:
Received 21 May 2011
Revised 3 October 2011
Accepted 12 October 2011
Available online 18 October 2011

Keywords:
Cratering
Ganymede
Impact processes

ABSTRACT

The morphology of impact craters on the icy Galilean satellites differs from craters on rocky bodies. The differences are thought due to the relative weakness of ice and the possible presence of sub-surface water layers. Digital elevation models constructed from Galileo images were used to measure a range of dimensions of craters on the dark and bright terrains of Ganymede. Measurements were made from multiple profiles across each crater, so that natural variation in crater dimensions could be assessed and averaged scaling trends constructed. The additional depth, slope and volume information reported in this work has enabled study of central peak formation and development, and allowed a quantitative assessment of the various theories for central pit formation. We note a possible difference in the size-morphology progression between small craters on icy and silicate bodies, where central peaks occur in small craters before there is any slumping of the crater rim, which is the opposite to the observed sequence on the Moon. Conversely, our crater dimension analyses suggest that the size-morphology progression of large lunar craters from central peak to peak-ring is mirrored on Ganymede, but that the peak-ring is subsequently modified to a central pit morphology. Pit formation may occur via the collapse of surface material into a void left by the gradual release of impact-induced volatiles or the drainage of impact melt into sub-crater fractures.

1. Introduction

As the Galilean satellites have a similar surface gravity to the Earth's moon, craters of the same diameter can be compared and used as a tool for comparing icy and rocky crusts. Craters on the icy Galilean satellites of Europa, Callisto and Ganymede exhibit the same simple and central peak morphologies seen for craters below 150 km on the Moon, but do not display the same peak-ring morphology as lunar craters above this diameter (McKinnon et al., 1991; Croft, 1985). Instead, large craters display characteristics with no obvious lunar analogues, such as central pits. The differences in the Galilean satellite and lunar cratering trends are considered to be due to the mechanical properties of ice or the presence of shallow sub-surface liquid layers (Moore et al., 2001; Turtle and Pierazzo, 2001; Schenk, 2002). Callisto is the most heavily cratered of the Galilean satellites, providing a rich collection of large impact craters for study. However, its surface has been found to be surprisingly crater-poor on smaller scales, leading Pappalardo (1999) to suggest that small craters are being erased more efficiently by mass wasting processes and burial by impact ejecta. Callisto is also thought to be less differentiated than Ganymede, leading to higher amounts of rocky material in its surface ice, which may affect its crustal strength properties in a way that would be difficult to predict. In contrast, the approximation of pure water ice for the surfaces of Europa and Ganymede is thought to be reasonable (Showman et al., 2004). As the ice crust of Ganymede is thicker than that of Europa, the morphologies of its smaller craters are expected to be less influenced by the presence of its sub-surface ocean (Schenk, 2002; Schenk et al., 2004). Ganymede therefore provides a suitable target for observations of craters that have formed in unlayered ice and thus a benchmark from which to understand craters in more complicated targets, such as Europa.

Images returned from the Voyager missions have allowed the analysis of crater morphology on the icy satellites and the construction of both diameter and depth-related scaling laws (e.g. Passey and Shoemaker, 1982; Schenk, 1991). Higher resolution Galileo data has since been used to update the diameter-related scaling trends (e.g. Schenk, 2002; Schenk and Ridolfi, 2002; Alzate and Barlow, 2011), and also crater depths on the basis of shadow measurements (Schenk, 2002).

* Corresponding author.
E-mail address: vjbray@lpl.arizona.edu (V.J. Bray).

0019-1035/$ - see front matter © 2011 Elsevier Inc. All rights reserved.
doi:10.1016/j.icarus.2011.10.004

Crater rim heights on the Moon and Ganymede, and consequently the crater depth, vary broadly with azimuth (Pike, 1977 *and references therein; this work*). Shadow length measurements are restricted to the line of illumination, providing one depth measurement and one rim height measurement per crater in each image. Scaling trends based on shadow length measurements therefore include significant uncertainties to account for natural variations in crater shape. Digital elevation models (DEMs) allow measurement of crater features from any part of the crater, and are not restricted to the line of illumination. Natural variation of crater shape with azimuth can thus be examined with the use of DEMs and used to calculate error bars on all measured values. Measurements from DEMs also add an important third dimension to other image-based data, providing slope information and allowing more accurate calculation of the volumes of particular crater features.

This work presents measurements of Ganymede crater dimensions and new volume calculations of central peaks, pits and pit-rims. Measurements were made from multiple topographic profiles extracted from DEMs created from Galileo Solid Sate Imager (SSI) images, so that natural variation in crater dimensions could be included in error measurements. A selection of these data was presented for central peak craters in Bray et al. (2008); this manuscript extends this dataset, re-assessing the main trends in crater dimensions and, in particular, focuses on the scaling trends of central pit craters.

2. Method

Digital elevation models (DEMs) presented in this work were created using both Stereo and Photoclinometric methods. Stereo-derived DEMs employed Galileo Solid State Imager (SSI) images and the stereo scene-recognition algorithms developed by Schenk et al. (1997) and Schenk and Bulmer (1998) which attempt to match albedo patterns in two stereo images of the same area, in patches of 5×5 pixels. The second technique, photoclinometry, is also known as "shape-from-shading" and derives the surface slope based on brightness variations from pixel to pixel. This method is complicated by the photometric nature of the surface (variations in albedo, etc.) and requires an accurate 'photometric function' to allow shade changes from topography to be differentiated from other surface effects. The photoclinometry-derived DEMs used in this work employed the line profiling tool described in Schenk (1989) and incorporate the combined lunar-Lambert photometric function as defined by McEwen (1991). Schenk (1989) notes that heights and slopes derived from this tool are accurate to better than 5% over distances of up to ~50 pixels. As the error in relative height determined from photoclinometry increases for length-scales of hundreds of pixels (Schenk, 1989), DEMs of large craters were never created by photoclinometry alone. Instead, the role of photoclinometry in the creation of large area DEMs was to sharpen the stereo-derived product (see Schenk et al., 1997). In this sharpening process the errors introduced over long distances no longer apply. DEMs of craters in this data set covered in high-albedo deposits (which also prove a source of error in photoclinometry) were produced with stereo only.

At least eight cross-sectional profiles were taken across each crater so that the natural variation of crater dimensions with azimuth could be included in the measurement error. Error bars included in Figs. 3–8 show the range of natural variation and incorporate a systematic error on depth measurements of ~5% (Schenk et al., 2004), an improvement from Voyager depth uncertainties of 10–30% (Schenk, 1991). Terrain type was noted during profile collection so that any differences in crater trends on bright and dark terrains could be documented.

We measured rim-to-rim crater diameter (D), depth (d), floor width (D_f), rim height (H_r), rimwall width (rw), average wall slope (S), central peak diameter, height and slope (D_{cp}, H_{cp} and S_{cp}), central pit diameter, depth and slope (D_p, d_p and S_p) and pit-rim diameter, height and slope (D_{pr}, H_{pr} and S_{pr}). Crater dimensions reported in this work (Fig. 1) were determined from an average of the measurements made from each cross-sectional profile. As a result, measurements presented here are less than

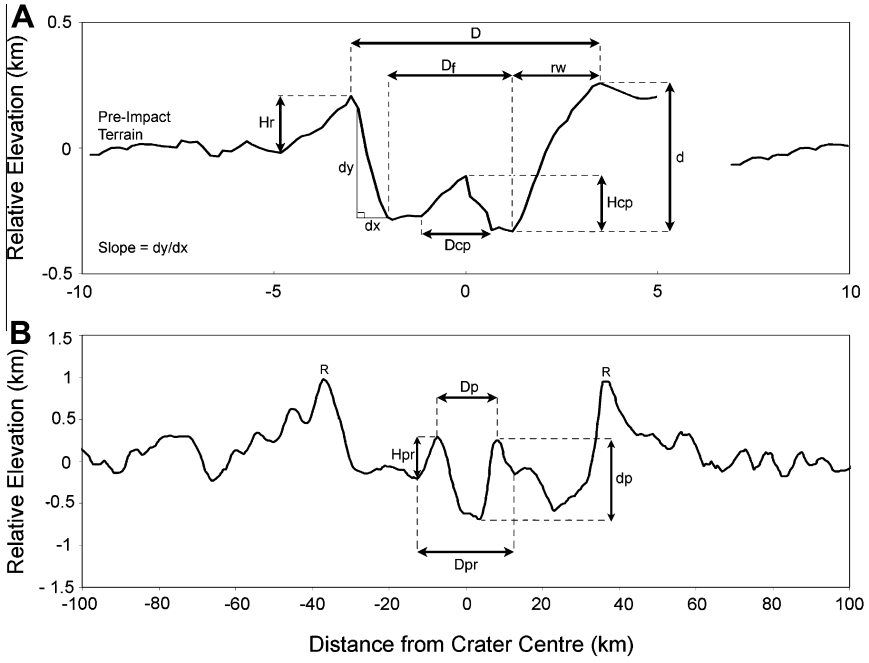

Fig. 1. Crater dimensions. Annotated profile of (A) a 7 km central peak crater at 23 N:194 W on Ganymede. Vertical exaggeration is 20:1. D is the rim-to-rim diameter; d is the rim to floor depth. Rim height and central peak height are noted with H_r and H_{cp} respectively. H_{cp} is central peak diameter. Wall slope calculation is also noted. (B) A 77 km central pit crater at 67.52S:201.48 W. Vertical exaggeration is 66:1. D, d, H_r and Wall slope were all measured as shown in (A). Additional measurement of pit diameter, pit depth, summit diameter and summit height are noted with D_p, d_p, D_s and d_s respectively.

established shadow-length derived depths, as these are maximum values (Schenk, 2002).

Central peak volumes were calculated from D_{cp} and H_{cp} measurements, assuming a conical shape. Central pit volumes were calculated in one of two ways, depending on their average cross-sectional shape: central pits with flat floors were approximated as a truncated cone; all other pit volumes were calculated assuming a simple conical shape.

Four small (D = 19.8–39.9 km) relaxed central pit craters with crater diameters below those of the fresh pit craters were included alongside the main dataset. This allows comparison of central pit craters formed during the current epoch with those formed during a time in Ganymede's history when conditions were perhaps more conducive to pit formation at smaller crater sizes. Also, where deemed appropriate, incorporation of these data into the main dataset allowed the extension of pit morphometry trends to smaller crater diameters.

3. Observations

3.1. Crater depths

Depth/diameter (d/D) ratios for fresh simple Ganymede craters were reported by Schenk (1991) to be similar to that of simple

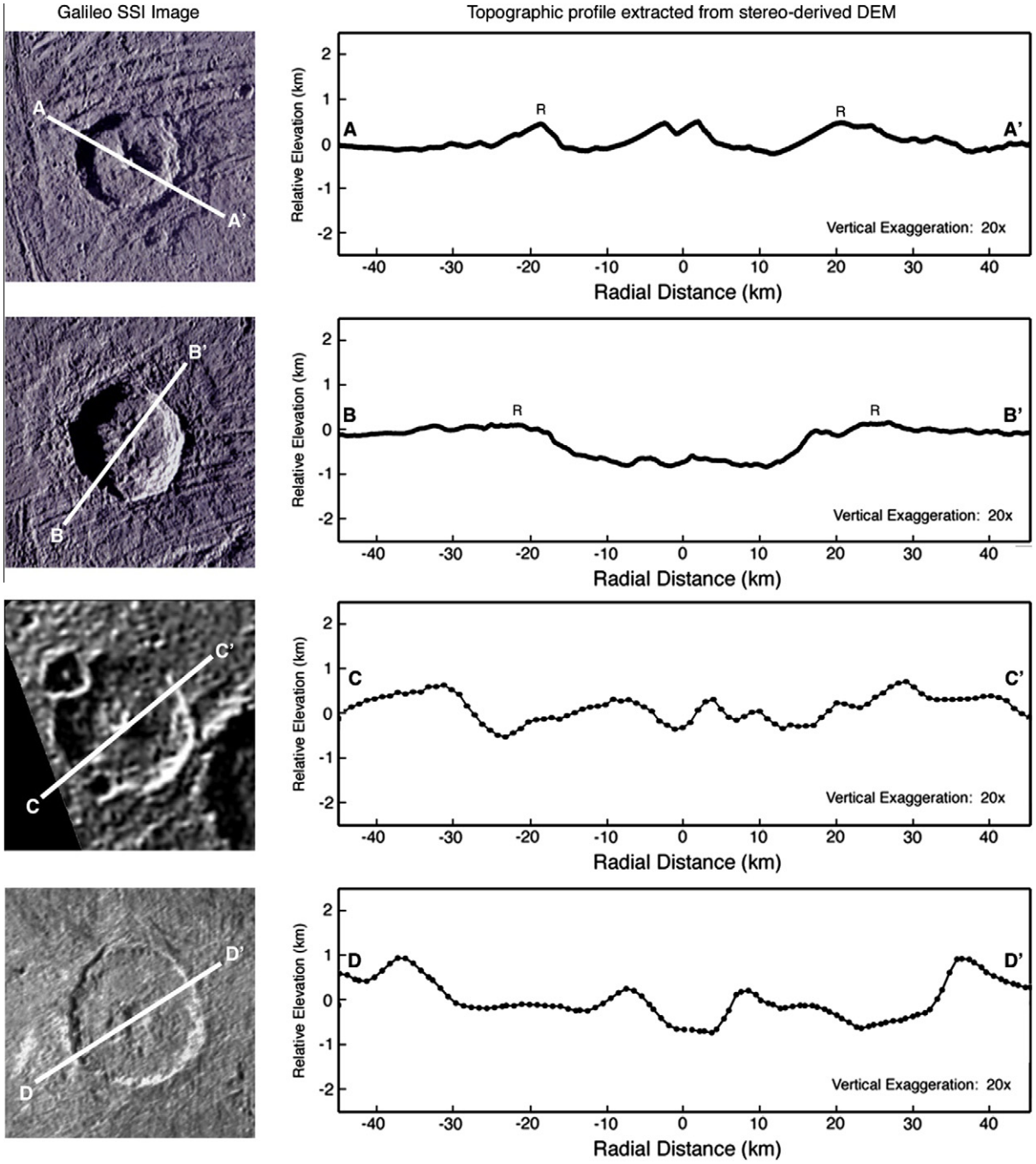

Fig. 2. Topographic profiles of transitional crater morphologies. Examples of the produced topographic profiles (right hand column). Galileo images are presented in the left column. The line along which the topographic profile was extracted is marked. (A) Example of 'transitional' morphology in a 39 km crater – pitted peak. (B) Example of 'transitional' morphology in a 42 km crater – hummocky floor. (C) Example of a 'tiered' central peak in a 51 km diameter crater. (D) Example of a flat-bottomed pit in a 77 km diameter crater.

lunar craters: $d/D \sim 0.2$. The depth of central peak craters on Ganymede increases with increasing crater diameter, to a similar degree as on the Moon – see solid lines in Fig. 3. However, complex craters on Ganymede are inherently 60–70% shallower than pristine lunar craters of the same diameter (Croft, 1981). The simple-to-complex transition diameter for craters on Ganymede is 1.9 ± 0.5 km (Schenk, 2002), much smaller than that on the Moon ($D \sim 15$ km (Pike, 1974)). Schenk (2002) also noted a transition at $D \sim 26$ km which is associated with a subtle decrease in crater depths and the transition from central peak to central pit morphology.

We measured the depth and diameters of 66 central peak, hummocky floored, pitted-peak and central pit craters on Ganymede ranging from 4.6 to 98.6 km in diameter (see circles and squares in Fig. 3). Crater depths are 0.34–1.65 km and generally increase with increasing crater diameter. This work does not include simple craters and only includes one data point for craters between 20 and 30 km in diameter; as a result, we do not comment on the simple-to-complex transition or the proposed transition at $D = 26$ km.

The central peak craters included in this work ($n = 25$) have depths from 0.34 (−0.06,+0.13) to 1.11 (−0.44,+0.32) km. The d/D ratio of central peak craters plots parallel to, but below, the established d/D trend for fresh craters from Schenk (2002) in Fig. 3A. This is expected to be due to the shadow-length derived depths in Schenk (2002) representing maximum depths. However, when maximum depth measurements of this work are employed (maximum error bars in Fig. 3A), they also plot below the trend established by Schenk (2002). This may be the result of footprint averaging of the stereo data – the smaller the crater, the smaller the number of pixels used to define the rim. This leads to averaging and loss of rim height, and thus a decrease in depth relative to the shadow length derived trend of Schenk (2002).

Hummocky-floored craters and those displaying pitted peaks ($n = 3$) have a diameter range of 34.8–50.1 km, and rim-to-floor depths ranging from 0.54 (−0.27,+0.21) to 1.46 (−0.19,+0.41) km. For the purposes of peak and pit morphometry comparisons, these intermediate/transitional craters are incorporated into the 'peak' dataset when the peak is the most prominent feature (Fig. 2A), and into the 'pit' group for the hummocky examples that have an apparent central pit (Fig. 2B).

Schenk (1991) notes constant or declining depths with crater size for central pit craters, with depths averaging 1.05 km and not exceeding 1.4 km. Our data set includes 38 central pit craters, including four obviously relaxed examples for comparison with the otherwise 'fresh' craters in the dataset. We report a near-constant average depth for the central pit craters included in this work ($d = 0.002D$), but also note a large scatter in central pit crater depths. Contrary to Schenk (2002), crater depth was not noted to decrease with increasing crater diameter. The relatively pristine central pit craters (subsequently referred to as central pit craters) have mean depths of 0.46 (−0.26,+0.17) to 1.65 (−0.37,+0.21) km, over a diameter range of 25.9–98.6 km. Relaxed examples have depths of 0.25–0.44 km for crater diameters of 19.8–39.9 km.

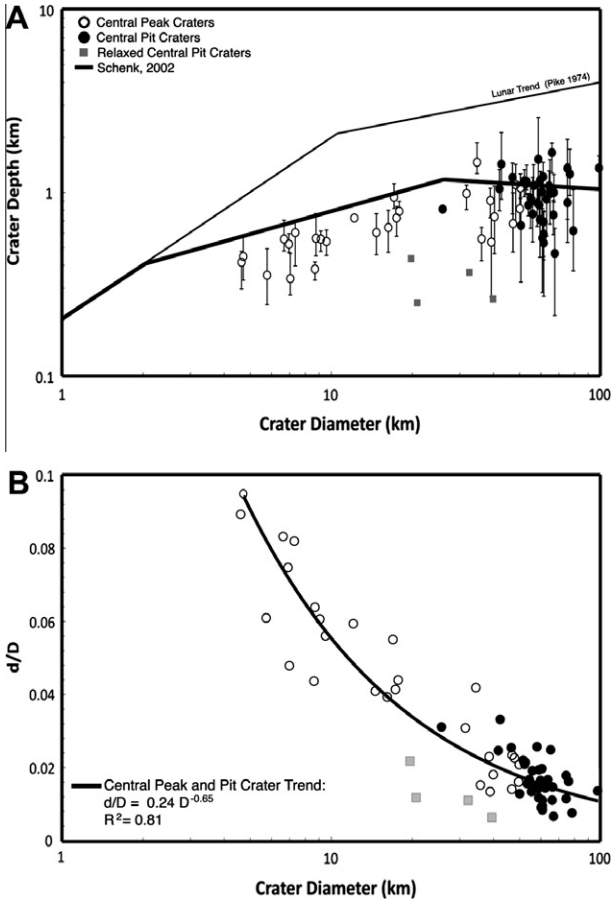

Fig. 3. Crater depths. Depth–diameter (d/D) relationships of Ganymede craters. (A) The average depth and diameter of craters measured in this work, compares to a lunar d/D trend line (Pike, 1974) and to a trend for the freshest of Ganymede craters (Schenk, 2002). (B) The decline in d/D with increasing crater size. The equation shown represents the d/D value of fresh craters only.

3.2. Wall slopes, rim heights, rimwall widths and floor widths

The wall slope and rim height of impact craters are useful dimensions in the study of large-scale movement and target material strength during impact crater formation: average wall slope can be used as a proxy for the effective target strength during crater formation, and rim height offers indirect evidence of the extent of crater wall collapse (Melosh, 1989; Schenk, 1991). Floor widths of lunar craters in a given size range tend to broaden with time (Baldwin, 1963; Pike, 1968, 1971). Average crater wall slopes are also noted to decrease with age (Head, 1975). Study of wall slope, rim height, rimwall width and floor diameter trends thus allows analysis of material movement during crater formation and the modification of crater morphology through continued rimwall collapse and other infill (e.g. deposition of ejecta from subsequent craters, etc.) over time.

Measurement of rim heights and wall slopes of Ganymede craters were reported and compared with lunar analogue values in Schenk (1991) and Bray et al. (2008). Fig. 4A and B show similar plots, this time presented so that differences between peak and pit craters are obvious; additional data points have been added to the Bray et al. (2008) dataset.

The average wall slope of central peak craters decreases from 24.5° to 3.6° for craters between 4.6 and 50.4 km in diameter. The average wall slope of central peak craters larger than $D \sim 36$ km remains approximately constant, at an average of ~5°. The wall slope of central pit craters, both fresh and relaxed examples, ranges from 2.48 to 17, with an average of 7.8°. The variation in crater wall slope with depth–diameter ratio is shown in Fig. 4A. Central peak crater wall slopes increase with increasing d/D ratio, following a power law. A trend for central pit craters was not identified due to the large spread of wall slope values, and the smaller d/D range that this crater type spans.

Fig. 4B shows the rim height of Ganymede craters, compared to a lunar trend based on data from Pike, 1977. Lunar crater rims increase proportionally with crater diameter until $D \sim 21$ km, when the H_r/D ratio decreases. This transition is thought to indicate significantly more collapse occurring in craters larger than 21 km in diameter and is associated with the simple-to-complex transition.

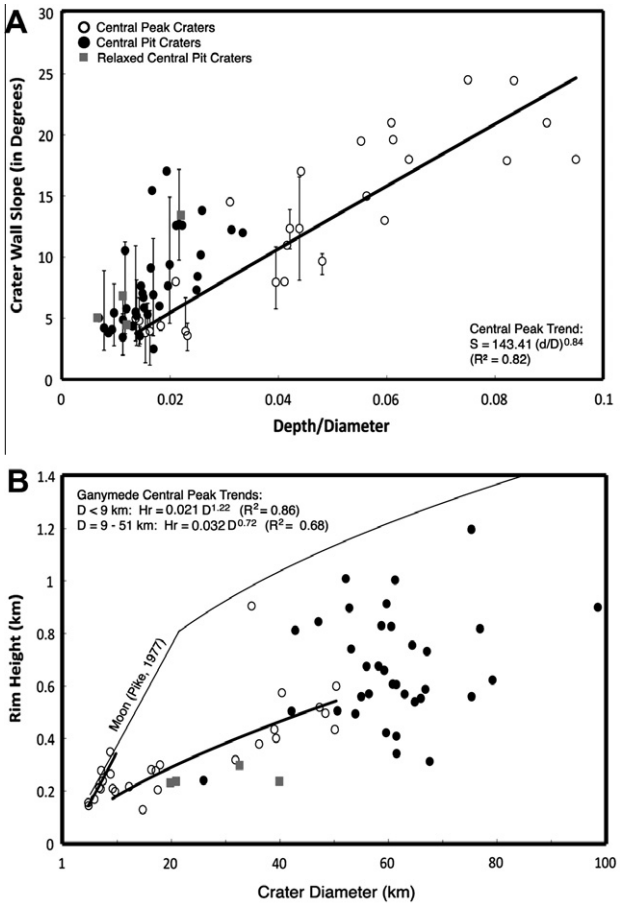

Fig. 4. Crater wall slopes and rim heights. (A) Crater wall slope values for craters with different d/D ratios. The relationship of central peak crater wall slope and d/D is noted with a trend line and the equation included in the plot. (B) Rim heights of Ganymede craters, compared to a lunar trend (thin black line). The two Ganymede trend lines (thick black line) were constructed from central peak crater measurements above and below $D = 9$ km.

A similar break in H_r/D trend was noted for Ganymede by Schenk (1991), occurring at $D \sim 14$ km.

This work notes that Ganymede craters below 9 km in diameter have similar rim heights to lunar craters. At $D \sim 9$ km, Ganymede crater rim heights decrease from ~0.35 km to 0.2 km. After this transition, rim height continues to increase with crater diameter at a slower rate than for $D < 9$ km. These separate relations from both Voyager (Schenk, 1991) and Galileo-based measurements are recorded in Bray et al. (2008). The range of rim heights for craters above 40 km in diameter is significantly larger than those below 40 km. For example, two $D \sim 70$ km examples have rim heights of 0.3 and 1.2 km. In addition to this variance from crater to crater, rim height is noted to be the most changeable dimension for any given crater, with a natural variation in rim heights with azimuth of 16–74%. Consequently, central pit craters display only a weakly positive trend with increasing crater diameter. The relaxed central pit craters are the smallest of the central pit craters included in this work, spanning crater diameters of 19–40 km, and have rim heights that lie on the main trend for craters between 10 and 40 km in diameter.

Normalized rim heights (H_r/D) of central peak craters decrease with growing crater diameter. At the morphological transition from central peak to central pit craters, normalized rim heights increase slightly from an average H_r/D of 0.01 to 0.015. Rim heights then remain constant (averaging $H_r = 0.67$ km) or decrease slightly.

Crater floor diameter increases with the increase in rim-to-rim diameter, following a power law fit to the combined dataset of central peak and pit craters (Fig. 5A). Craters less than 20 km in diameter have wider floors than for craters of comparable size on the Moon. Craters between 30 and 60 km in diameter on Ganymede have floor widths comparable to lunar craters of similar rim-to-rim diameters. At still larger crater diameters, Ganymede craters have up to 50% broader crater floors than craters of the same diameter on the Moon.

Rimwall widths in Ganymede central peak craters increase according to a power law (Fig. 5B). The trend in rimwall width is most obvious for craters below ~20 km in diameter. As the lunar trend used for comparison in Fig. 5B (Pike, 1977) applies only to craters above 15 km, we cannot directly compare the lunar and Ganymede trends for this range. For larger crater sizes, a correlation between rimwall width and crater diameter is less apparent and rimwall widths vary from 4.16 to 17.68 km, about an average of ~11 km. There may be a slight decrease in average rimwall widths for craters larger than $D \sim 60$ km, where Ganymede rimwall values consistently drop below the observed lunar trend. The smaller rimwall widths and correspondingly broader floor diameters of Ganymede craters of this size can also be noted by comparing the example topographic profiles in Fig. 6A and B. As the degree of collapse that occurs in a 60 km crater on Ganymede is expected to be equivalent to a much larger diameter crater on the Moon (Melosh, 1989), Fig. 6 also includes a larger lunar crater so that the rimwall width relative to the crater diameter can be

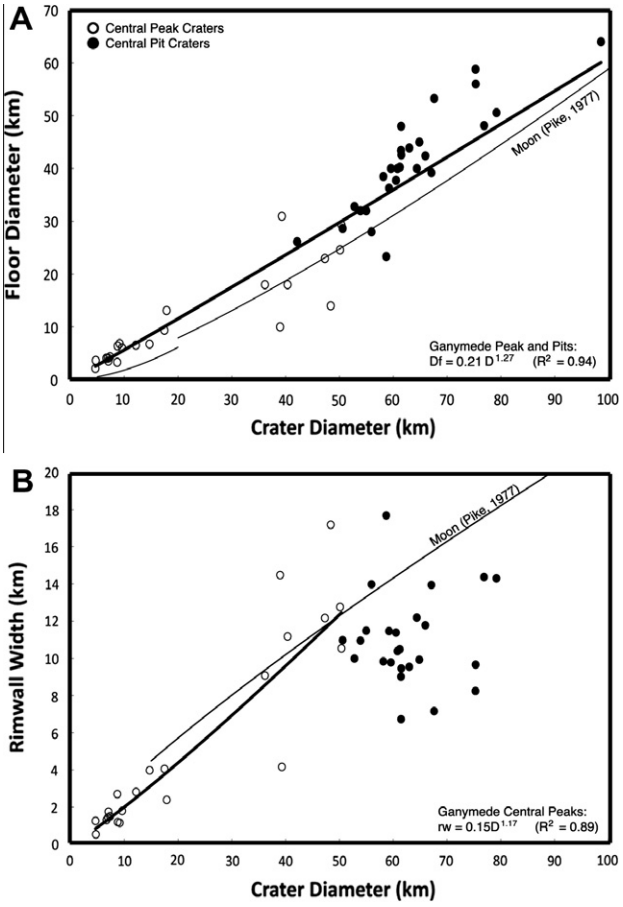

Fig. 5. Crater floor diameter and rimwall widths. (A) Ganymede crater floor diameters (data points and thick trendline), compared to a lunar trend (thin trend line). (B) Rimwall widths of Ganymede craters. The thick Ganymede trend line was constructed for central peak craters only. A lunar trend line (thin line) is included for comparison.

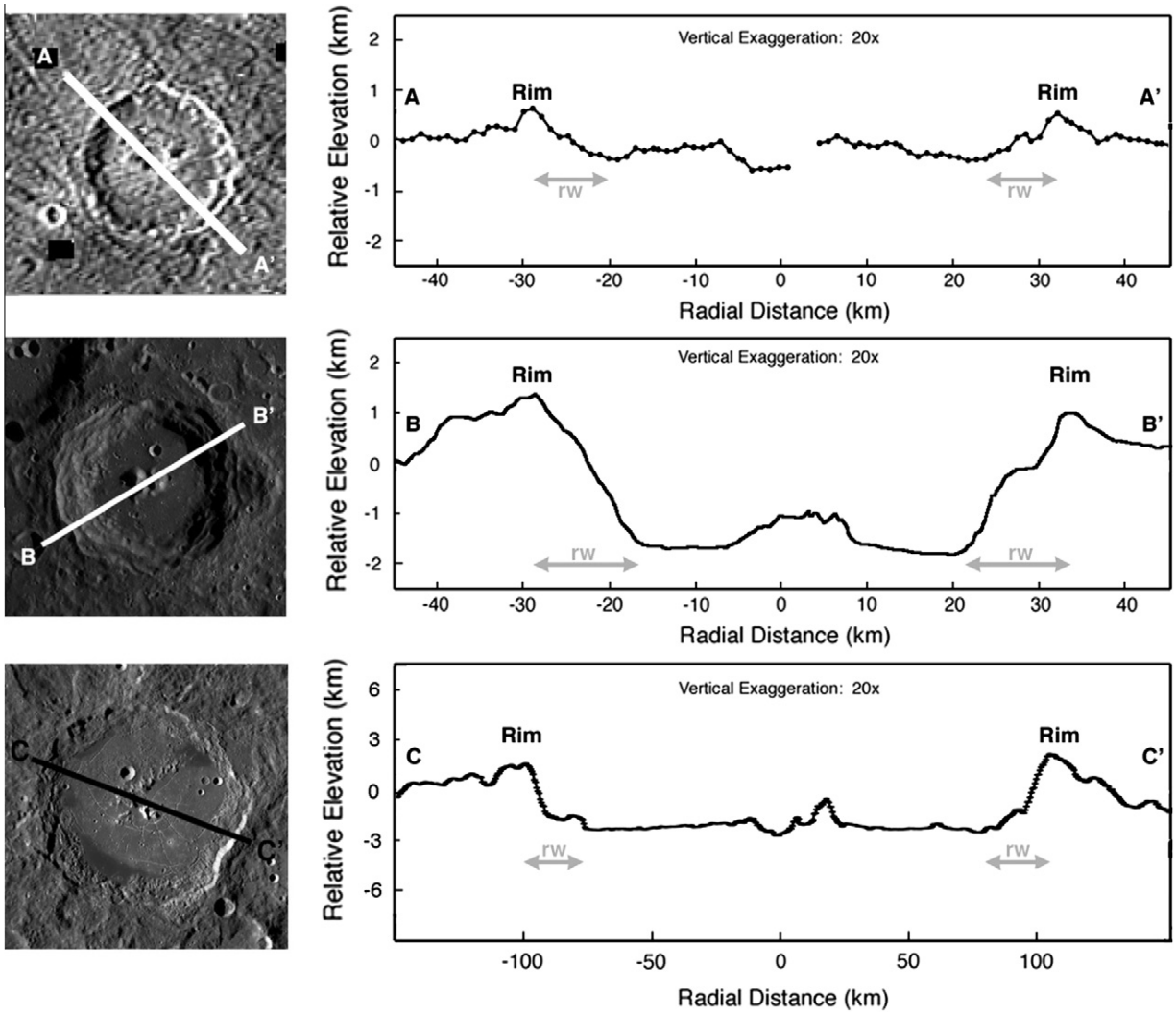

Fig. 6. Comparison of craters on the Moon and Ganymede. (A) Galileo image (left) of a 64.8 km diameter central pit crater on Ganymede (20.9°S:126.70°W), stereo-derived topographic profile (right). (B) Lunar Reconnaissance Orbiter Wide Angle Camera Image (left column) and Lunar Orbiter Laser Altimeter derived topographic profile (right column) of the 66.2 km diameter Bhabha crater on the Moon (55.1°S:−165°E). (C) Image and LOLA topographic profile of the 199 km diameter Humbolt crater on the Moon (27.2°S:80.9°E). Note different horizontal and vertical scales. The line along which each topographic profile was taken is marked on the images. Crater rims are indicated on each topographic profile and the width of the rimwall (rw) marked separately for the lunar and Ganymede cases with gray lines. Although the crater diameters are very similar, the Ganymede crater (A) has notably smaller rimwalls than a similar sized lunar crater (B).

compared in these different craters. Comparison of Fig. 6A and C show similar relative rimwall widths (normalized to crater diameter) in Ganymede craters of 60 km in diameter and lunar craters of ~200 km in diameter.

3.3. Peak and pit-rim dimensions

Central peak craters on Ganymede display two main peak morphologies – conical, and tiered (see Bray et al., 2008, Figs. 5 and 2C). Although suggested to be a morphological progression of peak shape with increasing crater size by Bray et al. (2008), acquisition of additional profiles suggests no obvious link of peak morphology with crater size, or terrain type. As a result, peaks with the typical conical morphology, and those with a two-tiered appearance have not been differentiated in the data plots.

Small pit craters on Ganymede tend to have raised rims around the central pits whereas larger floor pit craters have irregular broken pit-rims (Schenk, 1993). The dimensions of these rims have not yet been documented as their boundaries are poorly defined in images. The new topographic data acquired during the course of this work has allowed measurement of their dimensions. Comparison of the size-morphometry progressions of central peaks and peak-rings has added support to the hypothesis that peak-rings on silicate bodies develop from central peak collapse (Alexopoulos and McKinnon, 1994). Similarly, any common trends in the central peak and pit-rim size on icy bodies could suggest a link between these two morphological progressions. For this reason, although central peaks, and the rims surrounding central pits are morphologically distinct features, measurements of these dimensions have been plotted together in Figs. 3–6 so that any genetic relationship may be identified.

Central peak diameters (D_{cp}) have been noted to increase with crater size, according to the trends of Passey and Shoemaker (1982) ($D_{cp} \sim 0.3D$). We note a similar linear trend ($D_{cp} = 0.34D - 0.55$, $R^2 = 0.82$), but record a more confident fit for the central peak diameters in our dataset using the exponential equation: $D_{cp} = 1.99\exp(0.044D)$, ($R^2 = 0.87$). The pit-rim diameters in craters below 53 km in diameter also follow the central peak trend (Fig. 7A). At $D \sim 53$ km and $D_{cp} \sim 24$ km, the diameter of pit-rims increases at a greater rate, roughly following a linear trend: $D_{pr} = 2.79D - 125$ ($R^2 = 0.66$). The combined central peak and central pit-rim diameter trend can be described for craters up to 80 km

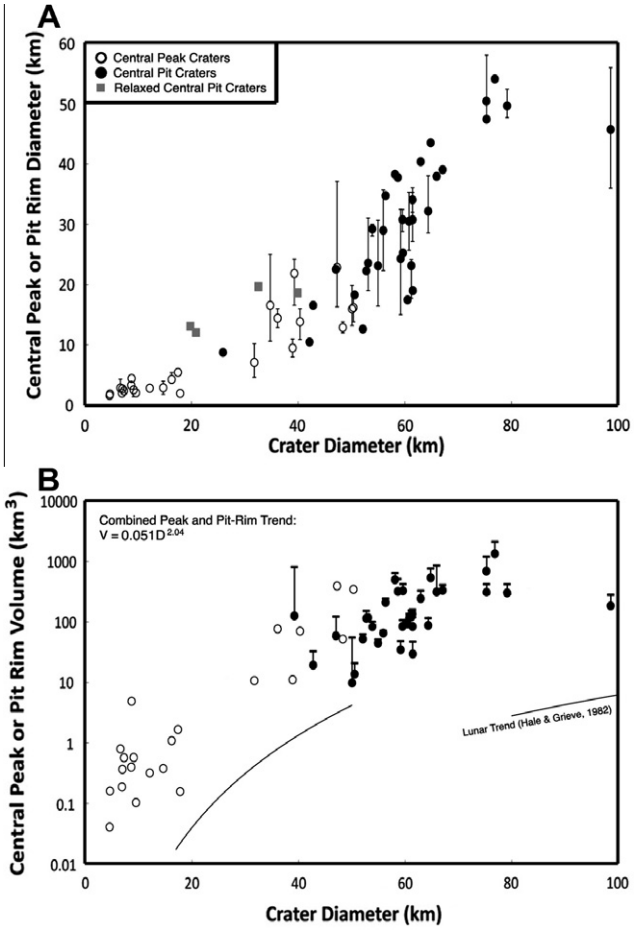

Fig. 7. Central uplift diameters and volumes. The size of central features of Ganymede craters. (A) The diameter of central peaks, and of pit-rims. (B) Volume of central peaks (white circles) and of pit-rims (black circles). The error bars on these data points represent the volume of the pit-rim and the pit it encloses, down to the crater floor level.

in diameter (D) with the single exponential relation: D_{cp} or $D_{pr} = 3.35\ \exp(0.036D)$. Relaxed central pit craters have larger central feature widths than fresher craters of similar rim-to-rim diameters.

As noted in Bray et al. (2008), central feature heights generally increase with crater diameter, but are highly variable, not following the trend suggested by Schenk (1991). Central peak and pit-rim heights are generally ~200 m for craters up to ~50 km in diameter. Above this crater diameter, pit-rim heights show even less of a trend with crater size, varying from 200 m to 1 km for craters between 50 and 100 km in diameter. The average slope of central peaks and pit-rims both vary from ~15° to 1°. The smallest central peak craters have the sleepest slopes; craters above $D \sim 20$ km have average central uplift slopes of ~4°.

Ganymede central peak volumes (calculated assuming a conical shape with radius $D_{cp}/2$ and height H_{cp}) follow a similar trend to that noted for lunar craters by Hale and Grieve (1982), but are two orders of magnitude larger (Fig. 7B). Pit-rim volumes plotted in Fig. 7B represent the volume of the pit-rim above the crater floor. In order to investigate the possibility that the rims of central pits represent the outer edges of large central peaks that have 'lost' their central material, the volume of pit-rims was also calculated by assuming a truncated cone with a base of D_{cp}, a depth of H_{cp} and a top vertex of D_p (thus including the encompassed pit volume down to the level of the crater floor). These values are marked on Fig. 7B as maximum error bars extending from the actual pit-rim measurement data points.

The growth of central peak and pit-rim volumes with increasing crater size can be described approximately with a single power law: $V_{cf} = 0.051D^{2.04}$. Due to the massive size of the pit-rims relative to the pits that they encompass, inclusion of pit volume into the pit-rim calculation does not significantly affect results. Central peak and pit-rim (with pit) volumes can still be described with a single power law: $V = 0.061D^{2.10}$.

3.4. Central pit trends

Central pits display a range of morphologies: Small pits are generally conical in shape (although image resolution may influence this observation). As crater size increases, central pits begin to exhibit a flat-floored appearance, followed by hummocky pit-floors and the emergence of central domes (Schenk, 1993).

Central pits increase in diameter with increasing crater size, as noted previously by Passey and Shoemaker (1982), among others, who recorded a positive exponential trend of $D_p = 1.9\exp(0.023D)$. Pit diameters recorded in this work are in agreement with this trend, although our recorded pit diameters are slightly larger ($D_p = 3.23\exp(0.023D)$). Pit depths are more variable, ranging from less than 0.1 km to 1.3 km. A weak indication of pit depth increase with crater size has been noted from Voyager-based measurements ($n = 9$, Schenk, 1993). We also note a weak ($R^2 = 0.3$) positive relationship between d_p and D ($d_p = 0.0016D^{1.42}$). The trend is smooth, showing no obvious variations in d_p/D for different crater diameters.

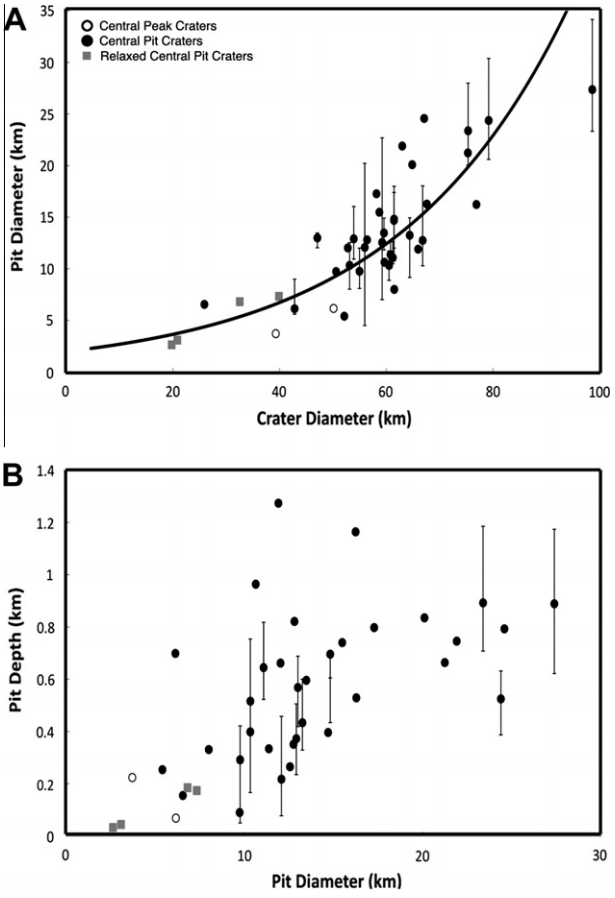

Fig. 8. Central pit diameters and depths. Central pit depth and diameter. (A) Pit diameter trend with crater diameter. Trend line is constructed using all data points. (B) Pit depth vs. pit diameters.

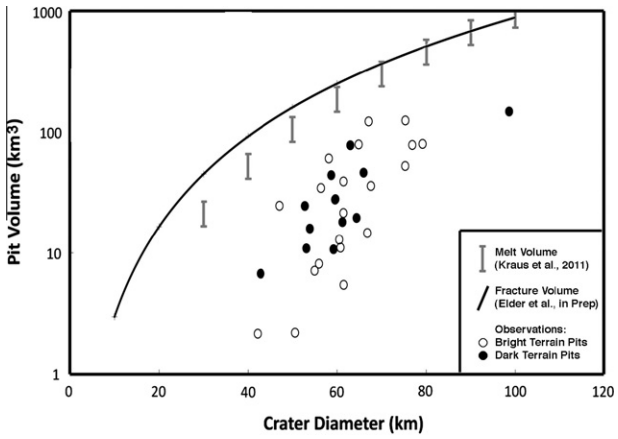

Fig. 9. Central pit volume and impact melt volume comparison. Pit volumes vs. crater diameter. Black and white circles mark measurements from pits in dark and bright terrains respectively. The trend line is constructed using data from both terrain types. Gray error bars mark the melt volume estimates for a 45°, 21 km s^{-1} impact into 110 K Ganymede surface ice using the scaling law defined in Kraus et al. (2011), assuming that 50–80% of melt remains in the crater after formation. The mass of vapor predicted by Kraus et al. (2011) is commonly two orders of magnitude less than the melt. The equivalent volume of the produced vapor under a range of pressure and temperature conditions remains in excess of the melt volume range shown here. Pit formation through the escape of impact-generated gases is thus also a viable formation mechanism based on the volumes of vapor involved.

There is however, a variation in d_p/D_p with crater diameter (Fig. 8C): pit depths generally increase with increasing pit diameter until a pit diameter of ~17 km is reached; pit depths then remain ~0.8 km. This apparent cut-off in vertical pit growth is reflected in a general increase in the percentage of 'flat bottomed' pits compared to the conical shapes seen in smaller pits (although both are present over a wide range of crater sizes). The slope of central pits ranges from 1.3° to 17.69° and shows no obvious trend with crater diameter. Relaxed central pit craters do not deviate from the main trends.

Central pit volumes were calculated in one of two ways, depending on their average cross-sectional shape: Central pits with flat floors were approximated as a truncated cone; all other pit volumes were calculated assuming a simple conical shape. Pit volumes increase with crater diameter (Fig. 9). The maximum pit volume recorded in this work is 151 km^3. No difference in pit volume was observed between pits in dark and bright terrain (Fig. 9).

4. Discussion

Measurements of the craters included in this work provide a representative sample of fresh crater morphometry on Ganymede. Here we discuss the implications of these observations (Tables 1–3) and use the derived trends in crater dimensions (Table 4) to investigate the different stages of the crater formation and modification process. The discussion is ordered in progressing stages of crater formation, and increasing crater diameter.

Possible differences in some peak and pit craters dimensions due to the (statistically likely) greater age of the pit craters are discussed. However, assessment of the effects of viscous relaxation on crater dimensions would require the acquisition of a comparable dataset of notably relaxed craters of similar diameters to the present fresher crater measurements. As this work only includes four obviously relaxed crater examples, and all at relatively small crater sizes, the effect of viscous relaxation on crater morphology is not fully discussed in this work.

4.1. Floor diameter variations and transient crater scaling

Estimates of transient crater dimensions are useful for assessing the depth of excavation of craters, and also necessary for melt volume estimates. A simple relation between final and transient crater dimensions can be derived assuming that the transient rim volume equals the transient crater volume, and that a transient crater of depth d_t and diameter D_t collapses in such a way as to conserve the volume of the material surrounding it. $D_t^3 d_t$ can then be calculated from measurements of final crater diameter, depth and floor diameter (Melosh, 1989). The existence of scaling laws for crater depth and floor diameter thus allow a simple scaling for transient crater dimensions with final crater diameter to be derived.

Although the general trend of floor diameters on Ganymede can be described well ($R^2 \sim 0.9$) using a single trend line, central pit craters above 60 km in diameter generally have broader crater floors than would be predicted based on the progression of D_f with D in smaller craters (Fig. 5A). As rimwall width increases with crater size until the development of central pit craters, but crater floor diameters continue to increase (Fig. 5), it could imply that at the crater size in which central pit craters occur rimwall development ceases, capped at a maximum width of ~18 km, or that the base of the rimwalls are being overlain by impact melt or debris from further rim collapse, for example. Statistically, the larger craters on a planetary surface are likely to be older than the smaller examples. Over time, mass wasting of material from the rim crest to the base of the rimwall acts to increase crater diameters, decrease crater depths, decrease rim heights and increase crater floor diameters (Baldwin, 1963; Pike, 1968, 1971). The greater normalized floor width (D_f/D) in central pit craters may therefore be age-related. The average trend reported in Table 1 is thus considered to offer a reasonable representation of crater floor diameters in fresh craters.

Using the geometric model presented in Melosh (1989, p. 143) and assuming a d_t/D_t ratio of 0.27, we use the rim-to-floor depth scaling trend of Bray et al. (2008) ($d = 0.23D^{0.45}$ for D = 5–50 km), and the floor diameter trend from this work ($D_f = 0.21D^{1.27}$) to derive a theoretical scaling for the transient crater diameter (D_t) from final crater diameter (D):

$$D_t = 0.919D^{0.866} \quad (1)$$

This scaling is in close agreement with the final-to-transient diameter scaling derived from observations of lunar and terrestrial craters (Croft, 1985), Ganymede and Callisto observations (McKinnon and Schenk, 1995), and hydrocode results (Kraus et al., 2011).

4.2. Rim collapse and the simple-to-complex transition

The relative amount of rim collapse on the Moon and Ganymede has been considered previously (e.g. Schenk, 1993; Bray et al., 2008). Ganymede complex craters below ~9 km in diameter have rim heights similar to lunar simple craters of the same size, indicating a similar amount of rim collapse, despite craters of this size being of simple morphology on the Moon, and central peak craters on Ganymede. Craters larger than $D \sim 9$ km have smaller rim heights than lunar examples (Fig. 4B), suggesting significantly more rim collapse than is seen in lunar craters of the same size. The small number of relaxed craters included in the dataset have rim heights that plot with the main trend, indicating that the decline in crater rim heights for craters $D > 9$ km relative to lunar values is a primary feature of Ganymede craters, most likely due to the ice-rich target (as noted by Schenk (1991)), and not an age-related phenomenon. The greater rim collapse of icy craters inferred from crater rim heights is supported by generally broader floor

Table 1
The major crater dimensions.

Crater location		Terrain (dark D, bright B)	Diameter, D (km)	Depth, d (km)	Wall slope, S (°)	Rim height, H_r (km)	Rimwall width, rw (km)	Floor diameter, D_f (km)
Lat.	Long.							
12.8	189.3	D	4.64	0.42	21.00	0.15	1.26	2.13
11.4	191.5	D	4.71	0.45	18.00	0.14	0.53	3.65
12.3	190.1	D	5.78	0.35	19.62	0.17		
12.8	193.2	D	6.68	0.56	24.46	0.21	1.31	4.06
22.6	194.1	D	6.96	0.52	24.52	0.21	1.44	4.08
36.0	10.3	D	7.05	0.34	9.67	0.28	1.76	3.53
24.4	193.7	D	7.35	0.60	17.89	0.24	1.50	4.34
40.3	12.2	D	8.70	0.38	12.33	0.35	2.70	3.30
10.9	189.3	D	8.77	0.56	18.00	0.26	1.19	6.38
13.2	200.4	D	9.15	0.56	21.00	0.21	1.15	6.84
1.1	200.7	D	9.59	0.54	15.00	0.20	1.80	6.00
39.3	193.3	B	12.18	0.73	13.00	0.21	2.82	6.54
39.2	191.7	B	14.70	0.60	8.00	0.13	3.98	6.74
1.1	152.6	B	16.29	0.64	7.95	0.28		
50	192	B	17.10	0.94	19.49	0.27		
38.4	194.9	B/D	17.47	0.73	10.98	0.20	4.05	9.36
13.5	202.2	D	17.88	0.79	17.01	0.30	2.39	13.10
0.4	201.4	D	19.78	0.44	13.42	0.23		
41	195.4	D	20.85	0.25	4.46	0.24		
33	192	D	25.91	0.81	12.23	0.24		
1.4	203.5	D	31.78	0.99	14.52	0.32		
38.9	15.2	D	32.54	0.37	6.83	0.30	3.83	24.88
−26.2	144.5	D	34.76	1.46	12.34	0.90		
17.3	49.8	D	36.15	0.56	3.81	0.38	9.08	18.00
49.5	55.7	B	38.96	0.90	3.57	0.43	14.48	10.00
64.1	12.3	B	39.29	0.54	4.98	0.40	4.16	30.96
40.9	200	D	39.88	0.26	5.04	0.24		
20.8	46.1	B	40.35	0.74	4.38	0.57	11.18	18.00
61.8	11.7	B	42.13	1.05	7.31	0.50	8.01	26.12
21	124	D	42.81	1.43	11.99	0.81		
−30.9	169.7	B	47.08	1.21	10.18	0.84		
−9.4	50	B	47.29	0.68	4.78	0.52	12.17	22.96
49	57.7	B	48.37	1.11	3.94	0.49	17.19	14.00
−36.5	53.4	B/D	50.11	0.82	3.94	0.43	12.77	24.58
−83.1	197.7	B	50.37	1.06	8.00	0.60	10.54	29.30
−14.5	56.1	B	50.59	0.66	4.36	0.50	10.98	28.64
37.7	140.2	D	52.13	1.16	12.60	1.00		
−29.1	167.7	D	52.78	1.12	12.59	0.89	9.99	32.80
−25.3	145	D	53.12	1.15	12.68	0.74		
28.8	49	D	53.90	0.85	5.31	0.49	10.95	32.00
24.7	54.1	B	54.98	0.93	2.48	0.56	11.49	32.00
−33.6	50.1	B	55.96	0.76	5.50	0.67	13.98	28.00
−30.6	163	B	56.39	1.09	17.03	0.57		
−35.3	162.8	B/D	58.15	0.88	6.70	0.67	9.84	38.48
−8.5	121.3	D	58.70	1.52	13.82	0.83	17.68	23.33
31.8	51.3	D	59.22	0.85	3.55	0.66	11.47	36.28
−20.3	55.7	B	59.56	0.71	5.78	0.42	9.78	40.00
35.2	141.4	D	59.65	1.17	7.65	0.91		
0.2	152	B	60.51	1.01	15.45	0.82	11.39	37.74
−4	46	B/D	60.78	0.56	4.07	0.60	10.39	40.00
−29.5	143	D	61.22	1.22	9.39	1.00	10.49	40.25
−5.9	53.4	B	61.44	0.69	3.44	0.60	9.02	43.40
−0.6	56.5	B	61.45	0.59	5.43	0.41	6.73	48.00
−18.7	52	B	61.49	0.53	3.79	0.34	9.46	42.58
23.8	193.8	D	62.98	0.92	7.63	0.56	9.54	43.89
29.7	47.5	D	64.38	1.09	6.92	0.75	12.19	40.00
−20.9	126.7	B	64.85	0.98	5.85	0.54	9.93	44.99
16.3	124	D	65.96	1.65	8.42	0.55	11.78	42.40
59.5	54.5	B	66.81	0.75	4.88	0.58		
−84.3	192.9	B	67.60	1.00	7.03	0.73	13.95	39.20
2.1	57.3	B	67.60	0.46	5.02	0.31	7.16	53.28
−12.7	119.5	B	75.29	1.36	5.99	1.19	8.24	58.80
23.2	74.7	B	75.32	0.88	10.54	0.56	9.66	56.00
−67.5	201.5	B	76.88	1.26	9.11	0.81	14.38	48.13
59.3	49	B	79.18	0.62	4.20	0.62	14.30	50.58
34.1	51.2	D	98.59	1.36	5.20	0.89	17.30	64.00

diameters (Fig. 5A) and gentler wall slopes on Ganymede then on the Moon (Bray et al., 2008, Fig. 4).

The transition in rim height at $D \sim 9$ km (noted at $D = 14.2$ and 11.9 km by Schenk (1991) and Bray et al. (2008) respectively) suggests a strength threshold has been exceeded at $D \sim 9$ km on Ganymede. A similar transition in rim heights is noted for lunar craters at $D = 15$ km, and is associated with the simple-to-complex transition (Pike, 1977). The Ganymede H_r/D transition is separate

Table 2
Central peak characteristics.

Crater location		Terrain (dark D, bright B)	Diameter, D (km)	Peak diameter, D_{cp} (km)	Peak height, H_{cp} (km)	Peak slope, S_{cp} (°)
Lat.	Long.					
12.8	189.3	D	4.64	1.60	0.07	4.96
11.4	191.5	D	4.71	1.86	0.19	12.35
12.3	190.1	D	5.78			
12.8	193.2	D	6.68	2.85	0.26	11.09
22.6	194.1	D	6.96	2.00	0.18	7.80
36.0	10.3	D	7.05	2.70	0.14	5.65
24.4	193.7	D	7.35	2.37	0.32	14.36
40.3	12.2	D	8.70	3.30	0.08	3.51
10.9	189.3	D	8.77	4.43	0.43	12.49
13.2	200.4	D	9.15	2.53	0.27	8.64
1.1	200.7	D	9.59	2.05	0.09	4.57
39.3	193.3	B	12.18	2.81	0.11	2.94
39.2	191.7	B	14.70	2.89	0.12	3.56
1.1	152.6	B	16.29	4.27	0.11	2.45
50	192	B	17.10		0.20	5.46
38.4	194.9	B/D	17.47	5.45	0.08	1.43
13.5	202.2	D	17.88	1.96	0.16	6.84
1.4	203.5	D	31.78	7.09	0.23	4.23
−26.2	144.5	D	34.76	16.57	0.41	6.26
17.3	49.8	D	36.15	14.45	0.20	1.68
49.5	55.7	B	38.96	9.50	0.10	1.00
20.8	46.1	B	40.35	13.83	0.21	1.66
−9.4	50	B	47.29	22.84	0.26	1.82
49	57.7	B	48.37	12.88	0.19	2.44
−83.1	197.7	B	50.37	16.20	0.63	12.79

Table 3
Central pit and pit-rim characteristics.

Crater location		Terrain (dark D, bright B)	Diameter, D (km)	Pit diameter, D_p (km)	Pit depth, d_p (km)	Pit slope, S_p (°)	Pit-rim diameter, D_{pr} (km)	Pit-rim height, H_{pr} (km)	Pit-rim slope, S_{pr} (°)
Lat.	Long.								
0.4	201.4	D	19.78	2.63	0.03		13.10	0.31	3.83
41.0	195.4	D	20.85	3.08	0.04		12.06	0.21	27.34
33	192	D	25.91	6.55	0.16		8.75	0.05	
38.9	15.2	D	32.54	6.81	0.19		19.67	0.23	
64.1	12.3	B	39.29	3.71	0.22	5.47	21.86	0.60	6.61
40.9	200	D	39.88	7.33	0.17		18.62	0.09	
21	124	D	42.81	6.13	0.70	9.13	16.57	0.15	3.49
−30.9	169.7	B	47.08	12.99	0.57	9.59	22.55	0.23	6.47
−36.5	53.4	B/D	50.11	6.15	0.07	1.31	15.95	0.10	1.20
−14.5	56.1	B	50.59	9.73	0.09	1.48	18.31	0.08	1.88
37.7	140.2	D	52.13	5.40	0.25	14.16	12.63	0.65	15.07
−29.1	167.7	D	52.78	12.02	0.66	7.46	22.28	0.53	7.42
−25.3	145	D	53.12	10.32	0.40	11.05	23.59	0.65	4.45
28.8	49	D	53.90	12.91	0.37	4.28	29.22	0.26	1.96
24.7	54.1	B	54.98	9.76	0.29	2.48	23.12	0.24	1.95
−33.6	50.1	B	55.96	12.07	0.22	2.59	28.99	0.28	1.34
−30.6	163	B	56.39	12.80	0.82	6.17	34.76	0.52	2.69
−35.3	162.8	B/D	58.15	17.27	0.80	6.33	38.29	0.73	5.83
−8.5	121.3	D	58.70	15.48	0.74	7.57	37.79	0.43	4.79
31.8	51.3	D	59.22	12.55	0.27	2.27	24.30	0.42	1.29
−20.3	55.7	B	59.56	13.47	0.60	5.00	30.79	0.36	1.69
35.2	141.4	D	59.65	10.63	0.96	8.11	25.25	1.06	12.87
0.2	152	B	60.51	10.33	0.52	9.12	17.48	0.78	9.92
−4	46	B/D	60.78	11.37	0.33	3.24	30.52	0.35	2.23
−29.5	143	D	61.22	11.07	0.64	11.05	23.14	0.52	6.35
−5.9	53.4	B	61.44	14.69	0.40	4.14	34.09	0.33	1.93
−0.6	56.5	B	61.45	14.81	0.70	5.55	30.77	0.24	2.09
−18.7	52	B	61.49	8.00	0.33	3.13	19.00	0.58	2.93
23.8	193.8	D	62.98	21.90	0.75	6.92	40.39	0.38	2.68
29.7	47.5	D	64.38	13.25	0.43	4.62	32.18	0.20	1.70
−20.9	126.7	B	64.85	20.09	0.84	7.57	43.53	0.59	4.79
16.3	124	D	65.96	11.90	1.27	17.69	37.97	0.35	7.54
59.5	54.5	B	66.81	12.75	0.35	4.54			2.42
−84.3	192.9	B	67.09	24.57	0.79	6.12	39.07	0.71	3.67
2.1	57.3	B	67.60	16.27	0.53	5.43			
−12.7	119.5	B	75.29	21.23	0.66	7.57	50.43	0.49	4.79
23.2	74.7	B	75.32	23.37	0.89	2.48	47.44	0.47	1.95
−67.5	201.5	B	76.88	16.23	1.16	9.52	54.12	0.84	6.34
59.3	49	B	79.18	24.37	0.52	2.94	49.65	0.29	1.80
34.1	51.2	D	98.59	27.37	0.89	6.43	45.74	0.24	1.69

from the s–c morphology transition at 1.9 ± 0.5 km (Schenk, 2002). This disparity has been used by Schenk (1991) and Bray et al. (2008) to suggest that the simple-to-complex transition at smaller crater diameters on icy satellites was more likely the result of rapid floor uplift due to weaker material at depth, rather than weaker surface ice allowing the onset of rim collapse at smaller crater diameters.

Measurement from higher resolution images of Ganymede craters could reveal an H_r/D transition associated with the s–c transition, as seen for lunar craters. However, until such data is available it appears that the lunar morphologic transition from simple craters to central peak craters via those with slumped walls and hummocky floors may be different on Ganymede. Current observations suggest that as Ganymede craters develop, central peaks occur at $D \sim 2$ km, leading to crater shallowing and a transition in d/D ratio due to floor uplift. Rim slumping then begins to occur noticeably at $D \sim 9$ km, leading to the H_r/D transition. Rim collapse should lead to a decrease in the d/D ratio, prompting another transition in the d/D trend. A distinct decrease in d/D at $D \sim 9$ km is not obvious from the current data (Fig. 3B).

4.3. Peak collapse and the development of pit-rims

The diameters of central peaks and pit-rims can be described using a single exponential equation. However, we note a kink in the data cloud of central feature width in Fig. 7A at $D \sim 53$ km. Below this transition diameter the central pit craters in our dataset ($n = 7$) have pit-rims with similar diameters to those that would be expected for a central peak in a crater of the same rim-to-rim diameter. The change in feature width trend therefore does not correspond directly with the peak-to-pit transition, but rather occurs at a slightly larger crater diameter.

The continuation of the central feature width trend across the morphological boundary, from central peak craters to central pit craters suggests a genetic relation between central peaks and central pit rims. The rims of central pits may therefore represent large central peaks that have continued to form in the same way as classical central peaks, but also incorporate a pit at the peak center. This seems particularly true for Mars where a higher percentage of pit craters are summit-pit craters (Barlow, 2010) in which the continuum from peak to summit-pit morphology is more obvious.

Normalized pit-rim diameters (D_{pr}/D) in craters above $D \sim 53$ km are greater than pit-rims and central peaks in craters $D < 53$ km. For central pit craters larger than ~53 km in diameter, the relatively large pit-rim diameters show that central pit-rims are not simply conical central peaks with a hollowed summit, but indicate that an additional process is occurring to widen the central crater features. This might be a consequence of pit formation that causes expansion, but does not immediately overprint the natural central uplift at small pit sizes. However, Fig. 7B shows that the increase in central peak and pit-rim volumes with increasing crater size can be described with a common trend. This shows that although the width of the central feature changes at $D \sim 53$ km, the volume does not show a similar increase after transition from central peaks to central pit craters. This suggests that expansion of the central area is not the cause of the broader pit-rims, and if expansion does occur in this region as a consequence of pit formation then it must do so without notable surface expression of the volume increase.

Relaxed central pit craters have larger central feature widths than fresher craters of similar rim-to-rim diameters (Fig. 7A). The process of viscous relaxation occurs faster in warmer targets (e.g. Thomas and Schubert, 1986). It is therefore a possibility that the additional heat at the crater center could lead to enhanced relaxation of the central regions of the crater floor without such a noticeable relaxed morphology for them to be classed as relaxed in this work. However, in order for the central portion to experience enhanced deformation, the material around it must be able to move to allow the deformation. This requires a similarly high temperature, which would facilitate relaxation of the whole crater (Dombard, personal communication). Additionally, viscous relaxation causes vertical displacement without significant lateral displacement. As no notable increase in pit-rim height or volume was noted at $D \sim 53$ km we do not consider accelerated relaxation of the central crater region to be the cause of the larger pit-rims in the large craters. Consequently, the broader pit-rims are considered to be a primary characteristic of the larger craters.

The increase in pit-rim width at $D \sim 53$ km could alternatively reflect the broadening of central uplifts (whether peaks, or pit-rims) due to collapse and outward spreading of the peak base of an overly large central uplift. The increasing degree of downwards and outwards collapse of central peaks as crater size increases has been described by Alexopoulos and McKinnon (1994), and collapse of the central uplift has been suggested as a mechanism for peak-ring formation on terrestrial bodies (e.g. Baldwin, 1981). We suggest that the same mechanism operates on Ganymede, forming features analogous to peak-rings. A later process, perhaps the drainage of the impact melt pool inside the peak-ring, then forms the central pit, over-printing the original peak-ring morphology. Such a progressive increase in the amount of peak collapse should be accompanied by either a leveling off or decline in central peak heights as crater size increases. Peak and pit-rim heights are extremely variable, preventing a clear trend in pit-rim heights from being established. This does not necessarily undermine the idea that pit-rims are the product of collapse of a central uplift. We suggest that any progression in peak-morphology (from conical, to those with a notably wider base due to basal collapse) such as that suggested for Ganymede by Bray et al. (2008), and for terrestrial bodies by Alexopoulos and McKinnon (1994) would be obscured by the results of variable impact velocity – faster impacts produce a more fluid central region, leading to less stable peaks which collapse into a tiered final morphology.

4.4. Pit dimensions and implications for formation mechanisms

The formation of central pits in impact craters remains a mystery, although several mechanisms have been proposed to explain them. The implications of our observations for the various theories are discussed in the following section. Acquisition of central pit profiles has enabled more accurate volume estimates than could be achieved with depth and diameter measurements alone. This information is useful for assessing the masses involved in the various pit formation processes and the influence of target properties on these different proposed processes.

No clear difference between the relative sizes of pits in different terrains was observed (Fig. 9), despite having been noted previously (e.g. Schenk, 1993; Klaybor and Barlow, 2006; Barlow, 2006). The presence of central pit craters on ice-rich bodies, but less notably in volatile-poor crusts, suggests that the pit formation mechanism is influenced by target material. The similar pit sizes in craters on dark and bright terrain therefore supports the hypothesis that the albedo difference between dark and bright terrain on Ganymede is not due to significantly increased rock content as suggested by Spencer (1987a). Instead, the darker terrain may be caused by a dark surface lag deposit of silicate material remaining after sublimation of the ice in an ice–silicate mixture (Spencer, 1987b). This, combined with the similarity of other crater dimensions in dark and bright terrain, supports the use of scaling trends derived from the combined data from craters on both dark and bright terrain.

4.4.1. Pit formation as a self-secondary

Some laboratory-scale impact experiments have shown that rising central peaks in multi-layered targets can become detached at

maximum elevation (Greeley et al., 1982). The debris from this disrupted peak then falls back into the original crater bowl creating a central secondary crater. Greeley et al. (1982) note that the secondary impactor created by the disruption of the central peak was most likely held together by surface tension in their laboratory experiments. As this property cannot be expected to scale to larger impact events, this theoretical pit formation mechanism is already deemed unlikely to operate on planetary scales.

Secondary craters close to the primary generally have shallower depths than a primary crater of the same size due to the lower impact velocity (Pike and Wilhelms, 1978). Such secondary craters therefore have lower d/D ratios. Formation of a secondary within the already impact-weakened and/or melted primary crater floor would also produce a shallower crater due to its formation in a weaker target. Comparing the depth–diameter ratio of central pits (d_p/D_p, Fig. 8B) to the depth–diameter ratio (d/D) that would be expected for a primary crater of $D = D_p$, our results show that central pits are not consistently shallower than an impact crater of the same size. This supports the conclusion of Greeley et al. (1982) that central pits are not formed through self-secondary impacts.

4.4.2. Impact into a layered target

Laboratory impact cratering experiments have shown that the presence of layering within a target has a direct effect on crater morphology at laboratory scales. Greeley et al. (1982) performed a series of gas-gun experiments into differently layered targets, which produced some crater forms deemed analogous to central pit craters. In that study, pits and 'disturbed' central terrain were created by high velocity impact into layers of water, clay, sand and ice in a variety of different layering combinations.

Investigation of this formation theory cannot be completed by analysis of observational data for Ganymede and instead requires different methods. Numerical modeling of impact into layered ice and water targets has not yielded any large final craters that have pitted centers (e.g. Bray, 2009; Senft and Stewart, 2011). The formation of large floor pits in Ganymede craters is thus not likely to be the result of sub-surface layering. It is plausible however, that the summit pit craters, more commonly seen on Mars, may be influenced by the transient cavity intersecting a layer of ground ice which then becomes a volatile center of a central peak. A secondary process such as sublimation or melt drainage would then be needed to form the pit.

4.4.3. Collapse of a central peak in weak ice

Passey and Shoemaker (1982) suggested that a central peak whose weight becomes too great to be supported by the subjacent material would promptly collapse during/after crater formation, creating a pit. It is not clear why such collapse is proposed to form a pit rather than centralized broken massifs as in the lunar crater Copernicus. However, if combined with the multiple peak oscillation theory of Melosh (1982), the development of a central pit might be possible in a target material acting as a Bingham fluid (a material that acts as a viscous fluid but has a definite plastic yield stress (Bingham, 1916)) during impact. This work already suggests that the rims surrounding central pits might be formed due to the basal collapse and spreading of a central uplift. The question then remains: does the collapsing peak descend further, forming the pit itself? Or does the center of the descending central uplift form a melt pool that, through a later process (e.g. drainage of the impact), forms the pit and overprints what would otherwise resemble peak-ring morphology? Computer simulations by Bray (2009) and Senft and Stewart (2011) have both produced modeled craters with melt pools of widths approximately equal to the diameter of central pits on Ganymede. Neither work notes a central depression produced purely from central uplift collapse. In order to investigate any possible contribution to pit formation that the collapse of a central uplift might have, the structure of pit-rims themselves must be explored.

4.4.4. Release of volatiles

Wood et al. (1978) proposed that central pit crater morphology on Mars might be due to the interaction of an expanding transient cavity with a sub-surface layer or zone of ice. The near adiabatic compression and generation of heat during impact is hypothesized to result in the explosive decompression of sub-surface volatiles on release from this high pressure (Kieffer, 1977). The upper rock layers uplift to form a central peak, whilst the volatile material at the core of the peak is lost via vaporization (Wood et al., 1978). The remaining crust is then suggested to collapse into the void left by the vented volatiles, forming a pit (Hodges et al., 1980). Such a process could also explain the existence of small summit pits on the Moon (c.f. Allen, 1975) if impact occurs into a region with relatively high volatile content.

Explosive release of volatiles would likely result in fresh deposits around the pits. This variant of the volatile release formation theory can thus be investigated by visual inspection of imagery. Schenk (1993) notes no obvious albedo difference surrounding pits on Ganymede that would indicate a layer of fresher ice at the surface. Also, if pit-rims represent products deposited due to explosive release of gases, then pit-rims should be of smaller volume than the pit. Our data shows pit-rims to be significantly larger than the pits they surround, indicating that they are not composed purely of explosive deposits.

A more gradual release of volatiles and subsequent collapse of the overlying ice cannot be evaluated as a formation mechanism by our measurements of Ganymede craters, other than to note that central pit volumes are orders of magnitude smaller than the expected vapor volumes produced by impact (e.g. Kraus et al., 2011). Consequently, this formation theory must be considered theoretically. The High Resolution Imaging Science Experiment (HiRISE, McEwen et al., 2007a) has revealed morphological features of geologically young impact craters, including the identification of 'ponded pitted material', interpreted to be impact melt deposits (McEwen et al., 2007b; Tornabene et al., 2007). The pits in these deposits do not have obvious surrounding ejecta that would indicate an explosive or impact origin. They are thought to be formed by the collapse of surface material into a void created by the venting of volatiles (Tornabene et al., 2007) or the drainage of melt water (Bray, 2009). It is possible that a high enough concentration of these pits at the center of martian craters would produce, or contribute to the formation of central pits (Bray et al., 2009). Such a process would also be valid for the formation of pits and small-scale pitting in Ganymede craters. Smaller satellite pits are noted around the central pit in Fig. 2D and could reflect the coalescence of the smaller scale pits to form larger pits close to the crater center.

4.4.5. Draining of impact melt

Croft (1981) presented the idea that, given the correct dimension and orientation of sub-crater fractures, drainage of brecciated rock, ice and melt-water could produce a pits on crater floors. The highest density of impact-induced fractures occur at crater centers (e.g. Kenkmann, 2002), likewise, the largest pockets of impact melt are concentrated in the central regions (e.g. Grieve et al., 1977) leading to a maximum potential for melt drainage at the center of craters. The offset of some central pits from the geographic center of their host crater can be explained by redistribution of melt and the most brecciated region due to variance in impact angle, pre-impact terrain slope, etc.

Croft (1981) notes that this formation mechanism allows for the production of central pits readily in ice-rich bodies, while also explaining the occurrences of pitted-peaks on dry bodies such as

Table 4
Summary of Ganymede impact crater scaling trends from this work.

	Scaling of crater dimension with crater diameter, D, depth, d, or d/D ratio		1 Sigma errors on equation constants Linear: $ax + b$ Power: ax^b Exponential: $a\exp(bx)$	
	D range (km)	Equation	a	b
Depth–diameter ratio, d/D	4–100	$0.24D^{-0.65}$	±0.038	±0.062
Crater floor diameter, D_f	4–100	$0.21D^{1.27}$	±0.164	±0.190
Rimwall width, rw	4–50 (central peak craters only)	$0.15D^{1.17}$	±0.165	±0.299
Crater wall slope, S	4–50 (central peak craters only)	$173.41\ (d/D)^{0.84}$	±128.23	±0.265
Rim height, H_r	$D < 9$	$0.021D^{1.22}$	±0.0248	±0.576
	$D = 9$–51	$0.032D^{0.72}$	±0.0227	±0.197
	$D > 51$	0.31–1.19 km		
Central peak diameter	4–50	$0.34D - 0.55$	±0.068	±1.746
		or		
		$1.99\exp(0.044D)$	±0.929	±0.0108
Pit rim diameter	50–100	$2.79D - 125$	±0.913	±50
Combined central feature diameter trend, D_{cf}	4–100	$3.35\exp(0.036D)$	±0.989	±0.0046
Central Peak or pit-rim volume	4–100	$0.051D^{2.04}$	±0.25	±1.16
Central pit diameter, D_p	<100	$3.23\exp(0.023D)$	±1.15	±0.0051
Central pit depth, d_p	<100	$0.0016D^{1.42}$	±0.00446	±0.648
Central pit volume, V_p	<100	$3.14D - 156.45$	±0.87	±55.07

the Moon (breccia drainage rather than melt drainage). However, drainage of brecciated material should theoretically lead to pits in all large lunar craters, not just those with central peaks. Bray (2009) suggests a similar theory, but restricts the draining material to actual molten products, be that rock-derived melt, or melt water. In the case of impact melt water draining through ice, the density difference between the solid and liquid phases will allow for the melt to force deeper into the sub-surface fractures, leading to the generally larger central pits observed on Ganymede, compared to Mars. Additionally, higher impact velocity and the target composition will produce more melt in the case of Ganymede (Bjorkmann and Holsapple, 1987; Pierazzo et al., 1997), providing a larger volume that can drain away, theoretically leading to larger pits than in martian craters.

Comparison of central pit volumes and expected melt and fracture volumes can provide a first-check of whether there is enough melt available in a crater of a given size to drain away, creating a void space of the order of the central pit volume. Fig. 9 includes estimated volumes of impact melt within different sized craters on Ganymede from the numerical work of Kraus et al. (2011). Error bars were used to mark the melt volume estimates of Kraus et al. (2011) as they consider a range of 50–80% of the original melt volume to remain in the crater cavity after excavation. Fig. 9 also includes the fracture space volume estimates of Elder et al. (in preparation), as the crater floor fracture volume dictates the maximum volume of melt that can drain from the surface melt pool. For crater diameters less than ~70 km the estimated fracture space is great enough to accommodate the full estimated melt volume. Above this crater diameter, some melt may not drain completely from the surface. The remaining undrained melt might then solidify as a pit floor pool, creating the flat floors noted most commonly in large central pits.

Both melt and fracture volume estimates are consistently larger than the pit volumes recorded in this work, showing there to be enough melt to theoretically drain away and cause a large pit. The smaller pit volumes compared with the melt and fracture volume estimates suggest that, if pits are formed by drainage of impact melt, then full drainage is not achieved, perhaps halting upon freezing shut of the fractures. This is the subject of the theoretical work of Elder et al. (2010, in preparation). The contrasting trend types (linear for pit volume, power law for melt and fracture volumes) suggest that if melt drainage plays a role in pit formation then there must be other factors influencing the pit volume. Additional influences may be related to the style and amount of crater floor fracturing, the thermal profile of the crater floor after each impact, and other factors that affect the volume of melt that can drain into sub-surface void space.

Observations and measurements of central pit craters can be used to further evaluate the validity of this formation mechanism in different ways: (a) by looking for evidence of drainage, or (b) by looking for evidence of the volume increase produced by recrystallization within the sub-crater fractures. Drainage channels and other such features are not confidently noted in Ganymede craters due to the relatively low resolution of Voyager and Galileo images. Investigation of channels and pitting within central pits on Mars (e.g. Bourke and Wray, 2011; Bray et al., 2009), at the higher resolution provided by the HiRISE (McEwen et al., 2007a) might record this process. However, collapse of overlying material, or of an ice crust formed atop an exposed surface melt pool, might then collapse into the void space created by drainage (Bray, 2009), obscuring direct evidence of that drainage.

The increase in pit-rim diameter at $D \sim 53$ km on Ganymede (Fig. 7A) might be a consequence of the expansion caused by recrystallization of melt water within fractures surrounding the pit from which it drained. It is possible that, in large impacts where sufficient melt is produced, the 9% volume increase produced by the recrystallization of melt water in the fracture space will cause some expansion and uplift of the central region. However, the lack of corresponding volume increase (Fig. 7B) of the central pit-rims suggests that if expansion does occur in this region as a consequence of melt drainage and recrystallization then it must do so without notable surface expression of the volume increase. This is not necessarily an impedance to this theory providing that the volume of melt water is able to sink straight down into the fractures, and not significantly into ice adjacent to the pit.

Alternatively, obtaining other geophysical data may help investigate this theory: Intense fracturing of the target during impact cratering results in a gravity low at the center of craters (Hildebrand et al., 1991). The recrystallization of impact melt water in fracture space will increase the density of the central region relative to the unfilled fractures further from the central pit. This mechanism of pit formation therefore predicts a concentric gravity low surrounding a relative gravity high over the very center of pit craters on Ganymede, and is thus a testable hypothesis.

4.5. A cap on pit depth and the development of domes

The decrease in d_p/D_p ratio at crater diameters of ~70 km (pit depth remains about constant at 0.8 km whilst pit diameter continues to increase, Fig. 8B) produces a change in the morphology of pit shapes, from conical to those with flat floors. Pit volumes may also begin to taper at this crater diameter (Fig. 9B). This may indicate a physical limit to the pit formation process, capping pit volumes at 151 km^3. For example, if applying the melt drainage model outlined in the last section then a decrease in d_p/D_p would imply that after some melt drained into fractures, either the fracture space became filled, or the melt had recrystallized in the fractures, preventing some of the melt from draining below the crater floor. This could lead to pooling of the remaining undrained melt at the floor of the pit, perhaps leading to the flat pit floors noted in craters larger than $D \sim 70$ km in this and other works.

Alternatively, cessation of pit volume growth could indicate that a separate process, such as dome formation, overprints the continued growth of central pits in the largest craters. The crater diameter at which this maximum in pit depths occurs corresponds roughly with crater diameters at which the emergence of central domes is noted (Schenk, 1993). It is therefore likely that the apparent cap on maximum pit depth is caused by the development of domes, raising the pit floors before the domes themselves can be seen in surface images.

If domes in central pit craters represent the uplift of relatively ice-rich material from depth as suggested by Schenk (1993), then the crater diameter at which d_p/D_p decreases can be used to estimate the depth to such a layer. Utilizing Eq. (1) and the general approximation that maximum depth of excavation H_{exe} is ~ equal to 1/10 of the transient crater diameter (Croft, 1980; Melosh, 1989), we estimate a depth of approximately 3.6 km to the proposed 'cleaner' ice layer. This is in accordance with the estimates of 3.5–4 km, based on applying terrestrial uplift depth estimates to central pit craters (Schenk, 1993), and 5 km from analysis of palimpsest stratigraphy (McKinnon and Parmentier, 1986).

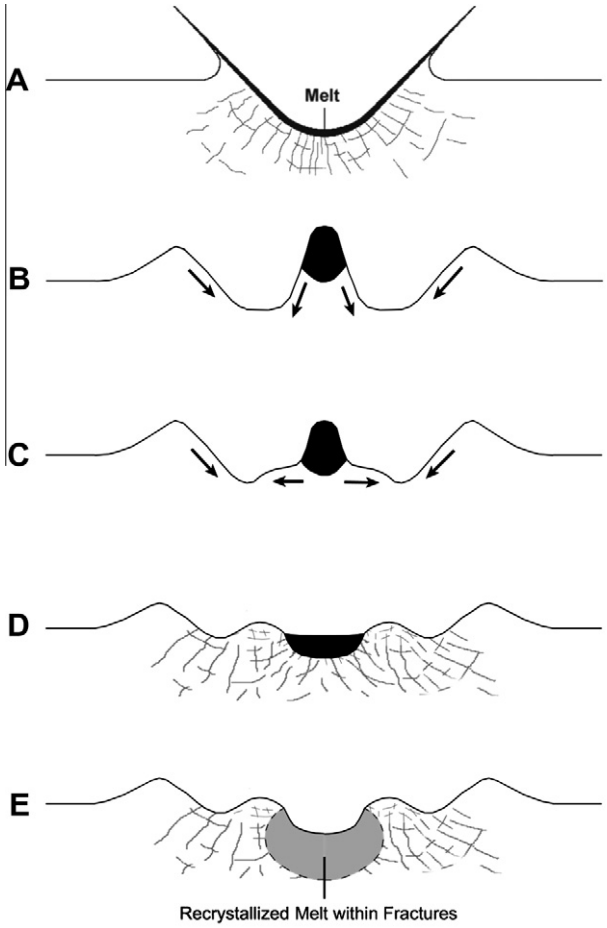

Fig. 10. Pit and pit-rim formation via central uplift collapse and melt drainage. Series of diagrams illustrating the formation of a floor pit crater using a combination of the melt-drainage and vapor release models. (A) Target is fractured and melted during impact. (B) Most melt is concentrated at the crater center, comprising a large part of the central uplift. If the uplift becomes too large to be supported by the subjacent material it will collapse. Modification of the crater rims by slumping is also occurring at this time. (C) The peak base collapses, spreading outwards. (D) Peak-rings are formed around a central melt pool. (E) The melt in the central region is removed, leaving a pit rather than a peak-ring structure. This loss is likely a combination of drainage of the melt into sub-surface fractures and loss of the most energetic material to space via evaporation and sublimation. Any crust that may have formed atop the melt pool due to the cold surface conditions at Ganymede will be thinned by further sublimation of the warm ice and through collapse into the void space created by drainage of the underlying melt.

5. Conclusions

Measurements of the craters included in this work provide a representative sample of fresh crater morphometry on Ganymede, allowing a relation between transient and final crater dimensions to be derived (4.1), and shedding light onto the formation and development of central peaks and central pits (4.2–4.4). The data has also exposed a possible difference in size-morphology progression between icy and silicate bodies, where central uplift begins to occur at smaller crater diameters than the initiation of rim slumping (4.2); this is opposite to the recorded lunar transition which notes the emergence of rim slumps first. This greater amount of central uplift is also reflected in the consistently larger central peaks on Ganymede, relative to lunar trends. Peaks increase in size as crater size increases, until the uplift is large enough to become unstable and collapse; the crater size at which the collapse of the central uplift occurs will be reduced in the case of impact conditions that may produce a weaker/more fluid central peak. We suggest that downward and outward collapse of unstable central uplifts on Ganymede forms features analogous to peak-rings on rocky bodies. A later process, perhaps the drainage of the impact melt pool inside the peak-ring, then forms a central pit, overprinting the otherwise peak-ring morphology. This suggested development is summarized in Fig. 10.

We noted no difference in pit dimensions on different terrains and consider the use of a combined dark and bright terrain dataset suitable for the analysis of central pit craters. The additional depth, slope and volume information reported in this work has enabled quantitative assessment of some of the central pit formation theories with regard to Ganymede craters (4.4). Pit morphology and depth–diameter ratios are not consistent with the idea of pit formation via self-secondary impact or explosive release of volatiles. Collapse of surface material into a void left by the gradual release of impact-induced volatiles or the drainage of impact melt into sub-crater fractures is considered to be a plausible formation mechanism for central pits on Ganymede given that the pit volumes are smaller than the expected amounts of melt and vapor produced by impact. The intricacies of these models must be assessed theoretically rather than by examination of currently available observational data. An apparent maximum pit depth reached in craters larger than 70 km in diameter may add support to the melt-drainage model if it marks a volume beyond which melt cannot fully drain into the floor fractures, resulting in a flat melt pool on the pit floor. Or it could herald the emergence of domes, raising the pit floors before the domes themselves can be seen in surface images. Pit formation on Ganymede due to target layering or the collapse of a central peak cannot be assessed with current observational data alone, but are considered unlikely on the basis of

computer simulations reported previously. The possible excavation of sub-surface volatile layers is still considered important for the formation of peak-pits seen on Mars and less commonly on the Moon.

Acknowledgments

We thank two anonymous reviewers for their constructive comments, Catherine Elder and Jim McElwaine for their help during the revision of this manuscript. This work was funded by Imperial College and by grant #NNX08BA96G from NASA's Outer Planets Research Program. Gareth Collins was funded by NERC grant: NE/E013589/1.

References

Alexopoulos, J.S., McKinnon, W.B., 1994. Large impact craters and basins on Venus, with implications for ring mechanics on the terrestrial planets. In: Dressler, B.O., Grieve, R.A.F., Sharpton, V.L. (Eds.), Large Meteorite Impacts and Planetary Evolution. Geol. Soc. Am. Spec. Pap. 293, pp. 29–50.

Allen, C.C., 1975. Central peaks in lunar craters. Earth, Moon Planets 12 (4), 463–474.

Alzate, N., Barlow, N.G., 2011. Central pit craters on Ganymede. Icarus 211 (2), 1274–1283.

Baldwin, R.B., 1963. The Measure of the Moon. Univ. of Chicago Press, Chicago, Ill.

Baldwin, R.B., 1981. On the tsunami theory of the origin of multi-ring basins. Multi-ring Basins. In: Schultz, P.H., Merrill, R.B. (Eds.), Proc. Lunar Sci. Conf. 12A, 275–288.

Barlow, N.G., 2006. Comparison of Central Pit Craters on Mars and Ganymede. Mars Crater Consortium 9 (abstract).

Barlow, N.G., 2010. Central pit craters: Observations from Mars and Ganymede and implications for formation models. GSA Special Papers 465, 15–27.

Bingham, E.C., 1916. An investigation of the laws of plastic flow. US Bureau Stand. Bull. 13, 309–353.

Bjorkmann, M.D., Holsapple, K.A., 1987. Velocity scaling impact melt volume. Int. J. Impact Eng. 5, 155–163.

Bray, V.J., 2009. Impact Crater Formation on the Icy Galilean Satellites. PhD Thesis, Imperial College London.

Bray, V.J., Collins, G.S., Morgan, J.V., Schenk, P.M., 2008. The effect of target properties on crater morphology: Comparison of central peak craters on the Moon and Ganymede. Meteorit. Planet. Sci. 43 (12), 1979–1992.

Bray, V.J., Tornabene, L.L., McEwen, A.S., Mattson, S.S, 2009. Measurement of small-scale pits in the Corinto crater, Mars. Lunar Planet. Sci. 40. Abstract #1389.

Bourke, M.C., Wray, J.J., 2011. Interdune deposits suggest high ground water in an equatorial crater on Mars. Lunar Planet. Sci. 42. Abstract #2749.

Croft, S.K., 1980. Cratering flow fields: Implications for the excavation and transient expansion stages of crate formation. Proc. Lunar Sci. Conf. 11, 2347–2378.

Croft, S.K., 1981. Cratering on Ganymede and Callisto: Comparisons with the terrestrial planets. Proc. Lunar Sci. Conf. 12, 187–189.

Croft, S.K., 1985. The scaling of complex craters. Proc. Lunar Sci. Conf. 13. J. Geophys. Res. 90, C828–C842.

Elder, C.M., Bray, V.J., Melosh, H.J., 2010. Central pit formation in Ganymede craters via melt drainage. Lunar Planet. Sci. 41. Abstract #2519.

Greeley, R., Fink, J.H., Gault, D.E., Guest, J.E., 1982. Experimental simulation of impact cratering on icy satellites. In: Morrison, D. (Ed.), Satellites of Jupiter. University of Arizona Press, Tucson, Arizona, pp. 340–378.

Grieve, R.A.F., Dence, M.R., Robertson, P.B., 1977. Cratering processes: As interpreted from the occurrence of impact melts. In: Roddy, D.J., Pepin, R.O., Merrill, R.B. (Eds.), Impact and Explosion Cratering. Pergamon Press, New York, pp. 791–814.

Hale, W., Grieve, R.A.F., 1982. Volumetric analysis of complex lunar craters: Implications for basin ring formation. Proc. Lunar Sci. Conf. 13. J. Geophys. Res. 87, A65–A76.

Head, J.W., 1975. Processes of lunar crater degradation: Changes in style with geologic time. The Moon, vol. 12. D. Reidel Publishers, Dordrecht-Holland, pp. 299–329.

Hildebrand, A.R. et al., 1991. Chicxulub Crater: A possible Cretaceous/Tertiary boundary impact crater on the Yucatan Peninsula, Mexico. Geology 19, 867–871.

Hodges, C.A., Shew, N.B., Clow, G.D., 1980. Distribution of central pit craters on Mars. Proc. Lunar Sci. Conf. 11, 450–452.

Kenkmann, T., 2002. Folding within seconds. Geology 30 (3), 231–234.

Kieffer, S.W., 1977. Sound speed in liquid–gas mixtures: Water–air and water–stream. J. Geophys. Res. 82, 2895–2904.

Klaybor, K., Barlow, N.G., 2006. Interior morphologies of impact craters on Ganymede. Lunar Planet. Sci. Abstract #1360.

Kraus, R.G., Senft, L.E., Stewart, A.T., 2011. Impacts into H_2O ice; scaling laws for melting, vaporization, excavation, and final crater size. Icarus 214 (2), 724–738.

McEwen, A.S., 1991. Photometric functions fro photoclinometry and other applications. Icarus 92, 298–311.

McEwen, A.S. et al., 2007a. Mars Reconnaissance Orbiter's High Resolution Imaging Science Experiment (HiRISE). J. Geophys. Res. 112, E05S02. doi:10.1029/2005JE002605.

McEwen, A.S. et al., 2007b. A closer look at water-related geologic activity on Mars. Science 317 (5845), 1706–1709.

McKinnon, W.B., Parmentier, E.M., 1986. Ganymede and Callisto. In: Burns, J.A., Matthews, M.S. (Eds.), Satellites. University of Arizona Press, Tucson, pp. 718–763.

McKinnon, W.B., Schenk, P.M., 1995. Estimated of comet fragment masses from impact crater chains on Callisto and Ganymede. Geophys. Res. Lett. 22 (13), 1829–1832.

McKinnon, W.B., Chapman, C.R., Housen, K.R., 1991. Cratering of the uranian satellites. In: Miner, E.D., Matthews, L.D. (Eds.), Uranus. Univ. of Arizona Press, Tucson, pp. 629–692.

Melosh, H.J., 1982. A schematic model of crater modification by gravity. J. Geophys. Res. 87, 371–380.

Melosh, H.J., 1989. Impact Cratering: A Geological Process. Number 11 in Oxford Monographs on Geology and Geophysics. Oxford Univ. Press, New York.

Moore, J.M., Asphaug, E., Belton, M.J.S., Bierhaus, B., Breneman, H.H., Brooks, S.M., Chapman, C.R., Chuang, F.C., Collins, G.C., Giese, B., Greeley, R., Head III, J.W., Kadel, S., Klaasen, K.P., Klemaszewski, J.E., Magee, K.P., Moreau, J., Morrison, D., Neukum, G., Pappalardo, R.T., Phillips, C.B., Schenk, P.M., Senske, D.A., Sullivan, R.J., Turtle, E.P., Williams, K.K., 2001. Impact features on Europa: Results of the Galileo Europa Mission (GEM). Icarus 151, 93–111.

Pappalardo, R.T., 1999. Ganymede and Callisto. In: Beatty, J.K., Petersen, C.C., Chaikin, A. (Eds.), The New Solar System, fourth ed. Cambridge University Press, pp. 263–275.

Passey, Q.R., Shoemaker, E.M., 1982. Craters and basins on Ganymede and Callisto: Morphological indicators of crustal evolution. In: Morrison, D. (Ed.), Satellites of Jupiter. Univ. of Arizona Press, Tucson, pp. 340–378.

Pierazzo, E., Vickery, A.M., Melosh, H.J., 1997. A reevaluation of impact melt production. Icarus 127, 408–423.

Pike, R.J., 1968. Meteoritic Origin and Consequent Endogenic Modification of Large Lunar Craters – A Study in Analytical Geomorphology. Ph.D. Thesis, University of Michigan, USA.

Pike, R.J., 1971. Some preliminary interpretations of lunar mass-wasting process from Apollo 10 photography. Analysis of Apollo Photography and Visual Observations, NASA SP-232, 14–20.

Pike, R.J., 1974. Depth/diameter relations of fresh lunar craters: Revision from spacecraft data. Geophys. Res. Lett. 1, 291–294.

Pike, R.J., 1977. Size-dependence in the shape of fresh impact craters on the Moon. In: Roddy, D.J., Pepin, R.O., Merill, R.B. (Eds.), Impact and Explosion Cratering. Pergamon Press, New York, pp. 489–509.

Pike, R.J., Wilhelms, D.E., 1978. Secondary impact craters on the Moon – Topographic form and geologic process. Proc. Lunar Sci. Conf. 9, 907–909.

Schenk, P.M., 1991. Ganymede and Callisto: Complex crater formation and planetary crusts. J Geophys. Res. 96, 15635–15664.

Schenk, P.M., 1993. Central pit and dome craters: Exposing the interiors of Ganymede and Callisto. J. Geophys. Res. 98, 7475–7498.

Schenk, P., 1989. Crater formation and modification on the icy satellites of Uranus and Saturn: Depth/diameter and central peak occurrence. J. Geophys. Res. 94, 3813–3832.

Schenk, P.M., 2002. Thickness constraints on the icy shells of the Galilean satellites from a comparison of crater shapes. Nature 417, 419–421.

Schenk, P.M., Bulmer, M.H., 1998. Origins of mountains on Io by thrust faulting and large-scale mass movement. Science 279, 1514–1516.

Schenk, P.M., Ridolfi, F.J., 2002. Morphology and scaling of ejecta deposits on icy satellites. Geophys. Res. Lett. 29 (12), 1590. doi:10.1029/2001GL013512.

Schenk, P.M., McEwen, A., Davies, A.G., Davenport, T., Jones, K., 1997. Geology and topography of Ra Patera, Io, in the Voyager era: Prelude to eruption. Geophys. Res. Lett. 24, 2467–2470.

Schenk, P.M., Wilson, R.R., Davies, A.G., 2004. Shield volcano topography and rheology of lava flows on Io. Icarus. 169, 98–110.

Senft, L.E., Stewart, S.T., 2011. Modeling the morphological diversity of impact craters on icy satellites. Icarus 214, 67–81.

Showman, A.P., Mosqueria, I., Head, J.W., 2004. On the resurfacing of Ganymede by liquid-water volcanism. Icarus 172, 625–640.

Spencer, J.R., 1987a. Icy Galilean satellite reflectance spectra: Less ice on Ganymede and Callisto? Icarus 44, 99–110.

Spencer, J.R., 1987b. Thermal segregation of water ice on the Galilean satellites. Icarus 69, 297–313.

Thomas, P.J., Schubert, G., 1986. Crater relaxation as a probe of Europa's interior. J. Geophys. Res. 91 (B4), D453–D459.

Tornabene, L.L., et al. 2007. Impact melting and the role of subsurface volatiles: Implications for the formation of valley networks and phyllosilicate-rich lithologies on early Mars. In: Seventh International Conference on Mars. Abstract #3288.

Turtle, E.P., Pierazzo, E., 2001. Thickness of a Europan ice shell from impact crater simulations. Science 294, 1326–1328.

Wood, C.A., Head, J.W., Cintala, M.J., 1978. Interior morphology of fresh martian craters: The effects of target characteristics. Lunar Planet. Sci. 9, 3691–3709.